CORA Cork Open Research Archive
Cartlann Taighde Oscailte Chorcaí

Title	Size-tuneable synthesis of nickel nanoparticles
Authors	Donegan, Keith P.;Godsell, Jeffrey F.;Otway, David J.;Morris, Michael A.;Roy, Saibal;Holmes, Justin D.
Publication date	2012-01-11
Original Citation	Donegan, K. P., Godsell, J. F., Otway, D. J., Morris, M. A., Roy, S. and Holmes, J. D. (2012) 'Size-tuneable synthesis of nickel nanoparticles', Journal of Nanoparticle Research, 14(1), 670 (10 pp). doi: 10.1007/s11051-011-0670-y
Type of publication	Article (peer-reviewed)
Link to publisher's version	https://link.springer.com/article/10.1007/s11051-011-0670-y - 10.1007/s11051-011-0670-y
Rights	© Springer Science+Business Media B.V. 2012. This is a post-peer-review, pre-copyedit version of an article published in Journal of Nanoparticle Research. The final authenticated version is available online at: http://dx.doi.org/10.1007/s11051-011-0670-y
Download date	2026-11-01 11:08:14
Item downloaded from	https://hdl.handle.net/10468/6740



UCC
University College Cork, Ireland
Coláiste na hOllscoile Corcaigh

Size-Tuneable Synthesis of Nickel Nanoparticles

Keith P. Donegan[†,ϕ], Jeffrey F. Godsell[‡], David J. Otway[†], Michael A. Morris[†,ϕ], Saibal Roy[‡] and Justin D. Holmes[†,ϕ*]

[†]Materials and Supercritical Fluids Group, Department of Chemistry and the Tyndall National Institute, University College Cork, Cork, Ireland. [ϕ]Centre for Research on Adaptive Nanostructures and Nanodevices (CRANN), Trinity College Dublin, Dublin 2, Ireland.

[‡]Microsystems Centre, Tyndall National Institute, Lee Maltings, Cork, Ireland.

*To whom correspondence should be addressed Tel: +353 (0)21 4903608; Fax: +353 (0)21 4274097; Email: j.holmes@ucc.ie

Abstract

A facile method is described for synthesising nickel nanoparticles *via* the thermal decomposition of an organometallic precursor in the presence of excess *n*-trioctylphosphine as a capping ligand. For the first time, alkylamines with different chain-lengths were employed as size-limiting agents in this synthesis. A direct correlation is demonstrated between the size of the alkylamine ligands used and the mean diameter of the nickel nanoparticles obtained. The use of bulky oleylamine as a size limiting agent over a reaction period of 30 minutes led to the growth of nickel nanoparticles with a mean diameter of 2.8 ± 0.9 nm. The employment of less bulky *N*,*N*-dimethylhexadecylamine groups led to the growth of nickel nanoparticles with a mean diameter of 4.4 ± 0.9 nm. By increasing the reaction time from 30 to 240 minutes, while employing oleylamine as the size limiting agent, the mean diameter of the nickel nanoparticles was increased from 2.8 ± 0.9 nm to 5.1 ± 0.7

nm. Decreasing the amount of capping ligand present in the reaction system allowed further growth of the nickel nanoparticles to 17.8 ± 1.3 nm. The size, structure and morphology of the nanoparticles synthesised were characterised by transmission electron microscopy and powder x-ray diffraction; while magnetic measurements indicated that the particles are superparamagnetic in nature.

Keywords: nickel; nanoparticles; decomposition; alkylamine; diameter control; superparamagnetic

Introduction

Discrete magnetic nanoparticles are of significant interest to researchers from a number of disciplines owing to their potential use as active components in the areas of catalysis, data storage, high density recording media and biomedical and environmental applications (Zhu et al. 2010; Du 2008; Wang 2008; Xu and Sun 2007; Liu 2006). As the size of a metal nanoparticle is reduced, a critical volume is reached whereby it is no longer energetically favourable to sustain magnetic domain walls and the particle will become a single magnetic domain. At this point, the particle will transition from ferromagnetic to superparamagnetic behaviour. The critical domain for nickel has been reported to be approximately 55 nm (Lu et al. 2007), however, this is dependent on synthesis conditions, *e.g.* temperature, capping ligands *etc*. For example, Luo et *al.* synthesised 16 nm hexagonal close packed (hcp) nickel nanoparticles which demonstrated ferromagnetism (and a coercivity of 8 Oe) at 300 K, indicating that the particles with diameters below the theoretical single-domain boundary can still exhibit ferromagnetism (Luo et al. 2009). Thus, the size of nickel nanoparticles alone will not determine whether the particles are single- or multi-domain in nature.

As the dimensions of ferromagnetic nanoparticles are reduced to below their critical volume, and the superparamagnetic regime is reached, their thermal instability often renders them unsuitable for applications such as data storage and high density data recording. However, superparamagnetic nanoparticles have proven to be ideal for many biomedical applications. For example, the lack of significant inter-particle interaction, which superparamagnetic nanoparticles generally exhibit, can lead to the synthesis of stable ferro-fluids that can be injected into biological systems and manipulated by external fields. These superparamagnetic dispersions are currently finding applications in the areas of magnetic resonance imaging, cancer treatments (hyperthermia), biological and chemical sensing and targeted drug delivery (Liu and Tang 2010; Dave and Gao 2009; Hergt et al. 2006; Tartaj et al. 2003; Babes et al. 1999).

The synthesis of superparamagnetic materials for these applications has thus far, focussed on iron oxides, *e.g.* maghemite (Fe_2O_3) and magnetite (Fe_3O_4) (Vidal-Vidal et al. 2006; Roca et al. 2006; Roca et al. 2009). However, attention has recently turned to alternative systems and nickel nanoparticles encapsulated in block co-polymers or apo-ferritin have been examined (Bala et al. 2009; Galvez et al. 2006). For any potential biomedical applications, a reliable synthesis method in which the size of the nanoparticles can be controlled is of utmost importance. Current methods for the controllable synthesis of metal nanoparticles include chemical reduction, co-precipitation methods, microemulsion techniques, polyol processes and electrochemical techniques (Murray et al. 2001; Sun and Zeng 2002; Ahmed et al. 2009; Fievet et al. 1989; Pachon et al. 2006). Thermal decomposition techniques, however, have demonstrated the synthesis of metal nanoparticles with extremely low size distributions (standard deviations of less than 5 %); a vital statistic for any potential applications of metal nanoparticles (Park et al. 2005; Farrell et al. 2003; Yang et al. 2007b). Park et *al.* outlined a

relatively facile method for the synthesis of size-tuneable nickel nanoparticles *via* the thermal decomposition of a nickel-oleylamine complex in the presence of a phosphine. By varying the type of phosphine, the size of the nickel nanoparticles could be controlled (Park et al. 2005). The formation of nickel oxides from these particles was achieved simply by exposing these nickel nanoparticles to air. In this work, nickel acetylacetonate was dissolved in an alkylamine and injected into a hot solution of tri-octylphosphine. Under these reaction conditions, the alkylamine is expected to control the rate of nucleation, and thus the size, of the nickel nanoparticles. Excess tri-octylphosphine in the reaction solution will act as a capping ligand on the surface of the nanoparticles preventing further growth, agglomeration and most importantly, oxidation of the particles after their formation. Thus, particle size can be varied by carefully controlling the amount of nuclei present, their growth rate and the amount of capping ligand present in the reaction synthesis.

In this manuscript we report for the first time the use of different chain length alkylamines to manipulate the diameter of spherical nickel nanoparticles in the presence of a surfactant. A direct correlation is demonstrated between the choice of alkylamine in the reaction medium and the mean diameters of the spherical nickel nanoparticles produced. Nickel nanoparticles which exist in the hcp phase have been shown to have larger coercivities than similarly sized fcc nanoparticles at 5 K and blocking temperatures which are above room temperature (Luo et al. 2009). Thus, in order to ensure the successful synthesis of superparamagnetic rather than ferromagnetic nickel nanoparticles in this study, an excess of tri-octylphosphine was used as the capping ligand in the reaction mixture; which is expected to inhibit a phase transition from fcc to hcp nickel.

Experimental

Nickel (II) acetylacetonate (Ni_2(acac)), tri-octylphosphine ($C_{24}H_{51}P$), *N*,*N*-diisopropylethylamine ($C_8H_{19}N$), *N*,*N*-dimethylhexadecylamine ($C_{18}H_{39}N$) and oleylamine ($C_{18}H_{37}N$) were all purchased from Sigma and used without further purification. In a typical reaction, nickel acetylacetonate (0.256 g, 1 mmol) was dissolved in the alkylamine (11.2 mmols) and heated to 373 K under nitrogen. In a separate round-bottomed flask, tri-octylphosphine (2.5 ml, 5.6 mmol) was degassed briefly under nitrogen at 373 K, before being heated to 493 K for 10 min. The mixture of nickel acetylacetonate and alkylamine was then injected into the hot tri-octylphosphine and heated at 493 K for 30 min under nitrogen. During this process, the colour of the mixture changed from blue to black indicating the formation of nickel nanoparticles. After 30 min, the reaction mixture was allowed to cool to room temperature. Anhydrous ethanol (30 ml) was added to the solution to facilitate precipitation of the nickel nanoparticles. This solution was then centrifuged at 8000 rpm for 30 min. The black solid was removed from solution and re-dispersed in hexane (~ 20 ml). Ethanol was added to precipitate the nanoparticles and this solution was centrifuged once more. A black solid was obtained after centrifugation and was re-dispersed in hexane (~ 20 ml).

The size and morphology of the particles were determined by transmission electron microscopy (TEM) on JEOL 200 and JEOL 2100 instruments, both operating at 200 kV. The samples for microscopy were prepared by dropping the dispersion of nanoparticles in hexane onto a carbon-coated copper grid for TEM analysis.

X-ray diffraction (XRD) analysis of the nanoparticles were determined on a Phillips X'Pert X-ray diffractometer, with graphite monochromatised Cu Kα radiation (α = 1.54178 Å). To

prepare the sample for analysis, excess ethanol was added to the mixture of nanoparticles in hexane and this solution was dispersed onto a glass slide and allowed to dry. A scan rate of 0.025^{o} s^{-1} was applied to record the pattern in the range $2\theta = 20 – 85^{o}$.

The magnetic properties of the particles were measured using a Quantum Design MPMS-XL5 superconducting quantum interference device (SQUID). The powder samples were placed within a polyimide capsule and characterized with an applied field range of ± 5 T and over a temperature range of 300 to 2 K.

Results and Discussion

Table 1 outlines the experimental parameters employed in the synthesis of the nickel nanoparticles synthesised in this study. For all reactions, the amount of nickel precursor present was maintained at 1 mmol. The type of alkylamine was varied from oleylamine (Ni-1) to *N*,*N*-dimethylhexadecylamine (Ni-2) and *N*,*N*-diisopropylethylamine (Ni-3). When compared to the reaction parameters used in the synthesis of sample Ni-1, sample Ni-4 was synthesised employing a longer reaction time, with all other parameters kept constant; sample Ni-5 was synthesised employing a longer reaction time and higher reaction temperature; while sample Ni-6 was synthesised with an increased amount of *n*-trioctylphosphine present.

Table 1 Experimental conditions used in the synthesis of nickel nanoparticles

Sample Name	Size Limiting Agent	Molar Ratio to n-TOP	Temperature (K)	Time (Min)	Size (nm)
Ni-1	Oleylamine	1: 2	493	30	2.8 ± 0.9
Ni-2	*N*,*N*-dimethylhexadecylamine	1: 2	493	30	4.4 ± 0.9
Ni-3	*N*,*N*-diisopropylethylamine	1: 2	493	30	5.1 ± 0.6
Ni-4	Oleylamine	1: 2	493	240	5.1 ± 0.7
Ni-5	Oleylamine	1: 2	588	240	6.4 ± 0.5
Ni-6	Oleylamine	1: 2.8	493	30	17.8 ± 1.3

Figure 1 displays an XRD pattern acquired from nickel nanoparticles synthesised from the thermal decomposition of nickel acetylacetonate in 5.6×10^{-3} mols of tri-octylphosphine at 493 K, with oleylamine acting as the size limiting agent (Ni-1). The diffraction pattern exhibited three distinctive peaks at 44.4°, 51.7° and 76.3° 2θ degrees, which can be indexed to the (111), (200) and (220) reflections of fcc nickel. Subsequent nickel nanoparticles synthesised using N, N-hexadecylamine, and N, N-diisopropylethylamine as the size limiting agents, revealed similarly resolved XRD patterns, attributable to the fcc phase of nickel. Upon exposure to air nickel nanoparticles synthesised *via* thermal decomposition can potentially oxidise to NiO (Dharmaraj et al. 2006; Davar et al. 2009). No nickel oxide peaks were observed in the nickel nanoparticles synthesised in this work owing to the surrounding capping layer on the surface of the nanoparticles provided by the presence of the alkylamine and the excess tri-octylphosphine.

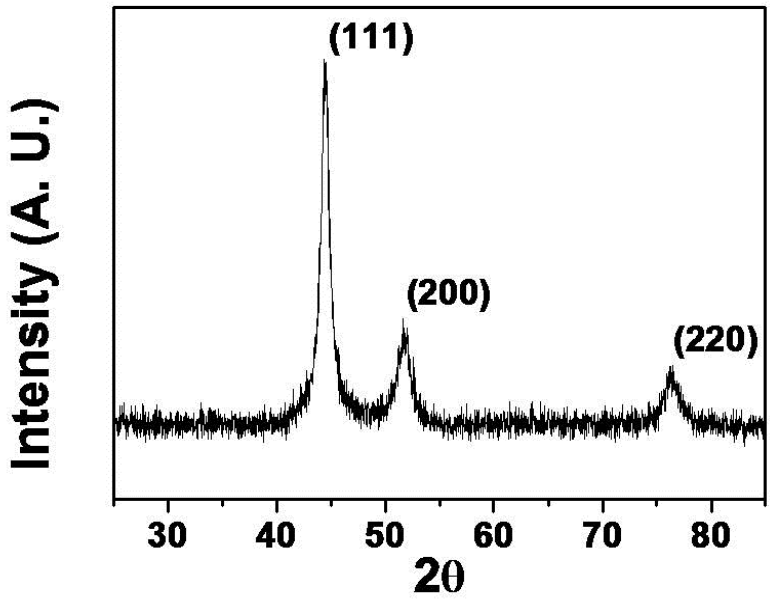


Fig. 1 XRD pattern of nickel nanoparticles synthesised at 493 K using oleylamine as a growth limiting agent, with 5.6×10^{-3} mol of tri-octylphosphine as the capping ligand (Ni-1)

Figure 2 displays TEM images of nickel nanoparticles obtained from the thermal decomposition of nickel acetylacetonate in tri-octylphosphine at 493 K using (A) oleylamine (Ni-1), (B) *N*,*N*-dimethylhexadecylamine (Ni-2) and (C) *N*,*N*-diisopropylethylamine (Ni-3) as the size limiting agent. Figure 2(D) shows the size distributions of each of the nickel nanoparticle samples. The mean diameters and standard deviations of the nickel nanoparticles synthesised were found to be 2.8 ± 0.9 nm, 4.4 ± 0.9 nm and 5.1 ± 0.6 nm for oleylamine, *N*,*N*-dimethylhexadecylamine and *N*,*N*-diisopropylethylamine, respectively.

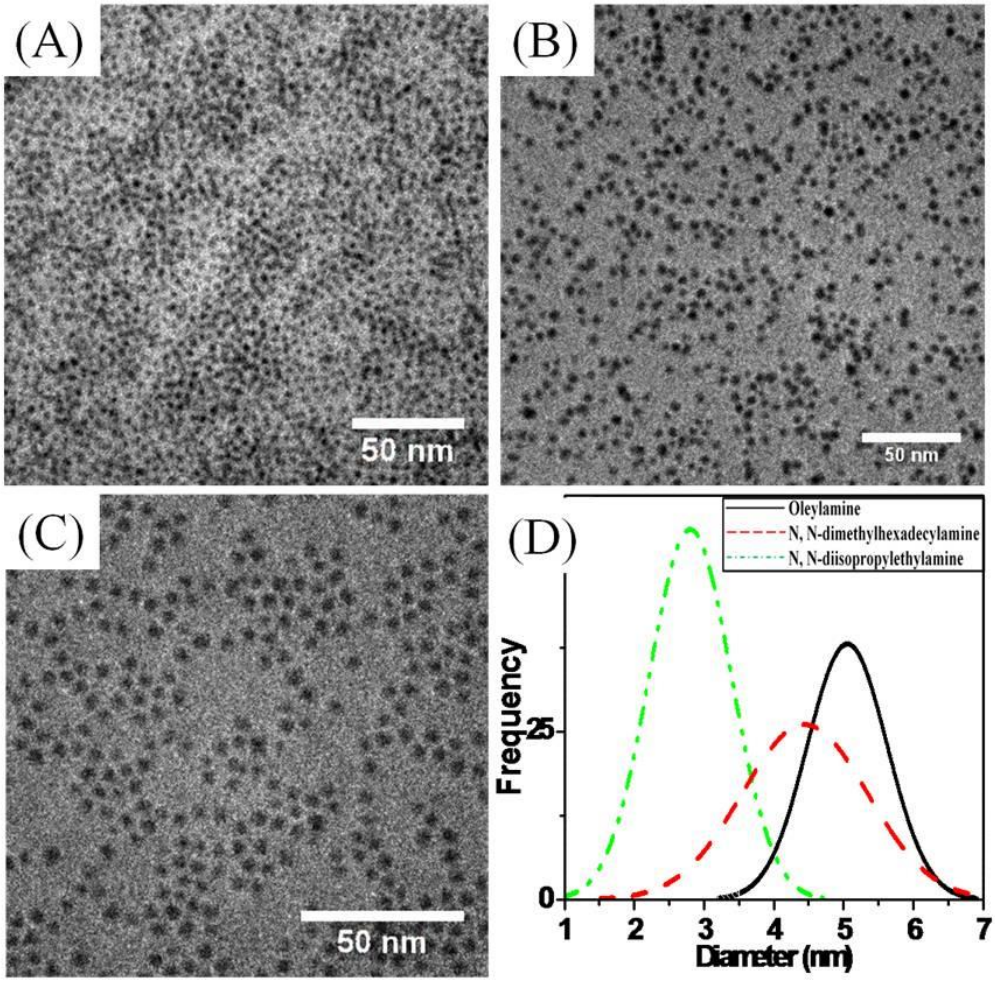


Fig. 2 Nickel nanoparticles synthesised at 493 K using (A) oleylamine (Ni-1), (B) N, N-dimethylhexadecylamine (Ni-2) and (C) N, N-diisopropylethylamine (Ni-3) as the size limiting agents. (D) Size distribution plots for the particles shown in (A), (B) and (C)

The nickel nuclei are generated upon decomposition of the nickel acetylacetonate. The size of the nanoparticles produced depends on the type of alkylamine used in the synthesis. The bulkiest amine chain is that of the oleylamine which is reflected in the smaller size of the nickel nanoparticles (2.8 ± 0.5 nm) formed using this alkylamine as the size limiting agent. The bulky nature of the oleylamine molecule limits the uptake of nickel nuclei into the nanoparticle core. A pattern was observed for the other alkylamines employed in this study, with the second longest alkylamine (the *N,N*-dimethylhexadecylamine) forming the second largest nanoparticles (4.4 ± 0.9 nm) and the shortest alkylamine (*N,N*-diisopropylethylamine) resulting in the synthesis of the largest nickel nanoparticles (5.1 ± 0.6 nm). Park et *al.* reported a similar correlation in the synthesis of nickel nanoparticles from nickel-oleylamine precursors. The larger, bulkier phosphines resulted in the synthesis of the smallest nickel nanoparticles; while the short chain phosphines resulted in the synthesis of larger nickel nanoparticles (Park et al. 2005).

The reaction mechanism for the formation of the nickel nanoparticles in this work is similar to that outlined for a number of nanoparticle systems outlined previously, including γ-Fe_2O_3, Fe_3O_4, and CoO (Hyeon et al. 2001; Yu et al. 2004; Zhang and Chen 2005). In each of these cases, a metal precursor is thermally decomposed in a solvent and subsequently capped using an acid (frequently oleic acid) or an alkylamine (usually oleylamine). In this work, nickel acetylacetonate is decomposed at temperatures above 493 K in various alkylamines which cap the metal particles and limit their growth, while tri-octylphosphine is subsequently employed as a stabilising ligand. A level of size control is thus demonstrated by varying the choice of alkylamine; and also by varying the time and temperature of the reaction.

Figure 3 displays nickel nanoparticles formed using oleylamine as the size limiting agent. The particles shown in Figure 3(A) are sample Ni-4 and were synthesised at 493 K with the reaction time increased from 30 to 240 min (corresponding nickel nanoparticles with a 30 min reaction time are shown in Figure 2 (A)). The size of these nanoparticles were found to be 5.1 nm ± 0.7 nm, which represents an increase in the mean diameter of 2.3 ± 0.2 nm from the particles synthesised with a reaction time of 30 min. Figure 3(B) displays a sample of Ni-5, which were the nickel nanoparticles synthesised using similar reactants as those shown in Figure 3(A), but with the temperature increased to 588 K (reaction time 240 min).

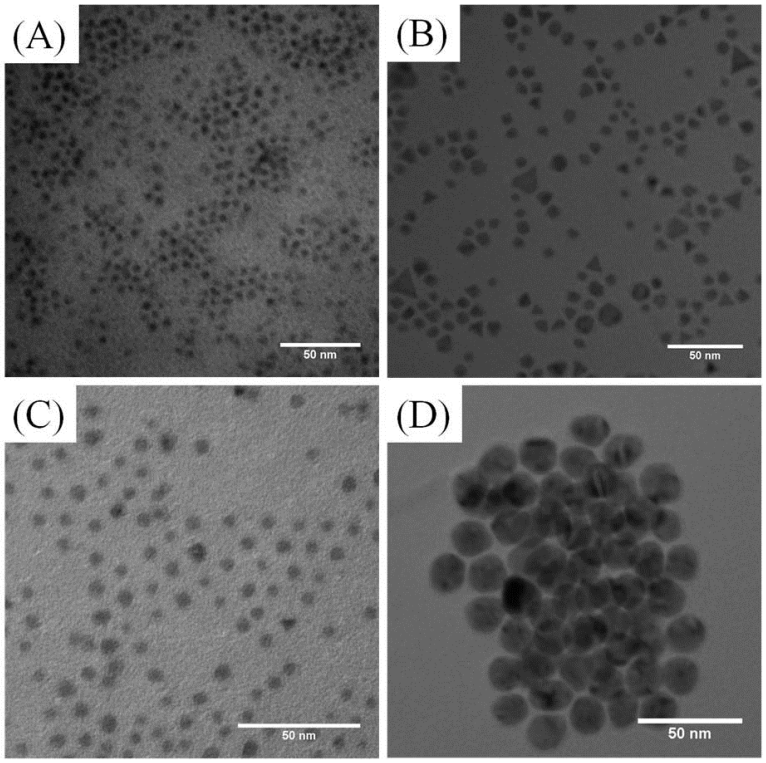


Fig. 3 (A) Nickel nanoparticles synthesised at 493 K for 240 min (Ni-4), (B) nickel nanoparticles synthesised at 588 K for 240 min, (C) particles removed by repeated centrifugation of (B) (Ni-5) and (D) nickel nanoparticles synthesised using 4×10^{-3} mol *n* -trioctylphosphine (Ni-6). All nanoparticles were synthesised using oleylamine as the size-limiting agent.

With increasing time and temperature, the emergence of nanoparticles in the shapes of hexagons and triangles were observable. Faceting of the edges of the particles was observed at these size domains owing to the growth of the particles via a ripening process. However, these larger particles could be removed by centrifugation. A solution of the nickel nanoparticles shown in Figure 3(B) were subjected to repeated centrifugation in order to remove the larger, poly-disperse nanoparticles. A solution of monodisperse nickel nanoparticles was obtained *via* this centrifugation process and these particles are displayed in Figure 3(C). The nanoparticles were found to have a mean diameter of 6.4 nm with a standard deviation of 0.5 nm. The nanoparticles in the TEM image were observed to organise into a hexagonal arrangement in some areas with the gaps between the particles assumed to comprise the capping ligands which could not be seen by TEM.

For the reaction mechanism outlined here, increasing the ligand concentration in the initial reaction solution, i.e. from 1: 2 for Ni-1 to 1: 2.8 for Ni-6, causes a reduction in the monomer activity. This results in the formation of fewer nuclei and thus, as Ostwald ripening continues, larger nanoparticles will grow. Thus, the size of the nanoparticles is observed to increase from 2.8 to 17.8 nm. In the case of magnetite (Fe_3O_4), Yu et *al.*(Yu et al. 2004) thermally decomposed FeO(OH) in the presence of oleic acid and 1-octadecence to demonstrate a size-controllable synthesis. Similar to the method outlined here for nickel nanoparticles, larger nanoparticles were formed by increasing molar ratio of ligand to precursor, by increasing the time of the reaction and by raising the reaction temperature. Similarly, Hyeon et *al.* (Hyeon et al. 2001) reported increasing sizes of maghemite (γ-Fe_2O_3) nanocrystallites *via* thermal decomposition of iron pentacarbonyl ($Fe(CO)_5$) with increasing ratios of ligand to precursor. While Zhang (Zhang and Chen 2005) outlined one of the more facile synthesis techniques in the preparation of CoO nanoparticles from the thermal

decomposition of cobalt acetylacetonate in oleylamine, where the size of the particles produced was controlled simply by varying the time and temperature of the reaction accordingly. Purely metal systems have similarly been prepared using the thermal decomposition method. Yang et *al.* thermally decomposed iron pentacarbonyl in the presence of oleylamine and kerosene (Yang et al. 2007a) in a glove-box to prevent oxidation; while cobalt nanoparticles passivated with oleic acid and tri-phenylphosphine have been synthesised *via* the thermal decomposition of dicobalt octacarbonyl (Yang et al. 2004).

A phase transition from fcc to hcp would be expected upon increasing the reaction temperature to 588 K, as this is a higher temperature than the 518 K postulated by Chen et *al.* at which the fcc nickel phase changes to hcp (Chen et al. 2007). There was a slight change in the XRD pattern obtained (Figure 4) for the nickel nanoparticles synthesised at 588 K compared to the nickel nanoparticles synthesised at 493 K. As seen in the XRD pattern of the nickel nanoparticles synthesised at 588 K (Figure 4), four distinct peaks are observed at 44.2º, 48.4º, 64.5º and 81.8º 2θ degrees. These peaks can be indexed to the (111), (200), (220) and (222) reflections of fcc nickel. Thus, an increase in the reaction time for the synthesis of nickel nanoparticles and increasing the reaction temperature, which had been reported by other groups to assist the phase transition of nickel nanoparticles, is not enough in this case to transform the fcc nickel nanoparticles to hcp (Chen et al. 2007). As mentioned above, this is most likely due to the presence of bulky alkylamines as size limiting agents and, more importantly, the presence of excess tri-octylphosphine as the sterically hindering capping ligand.

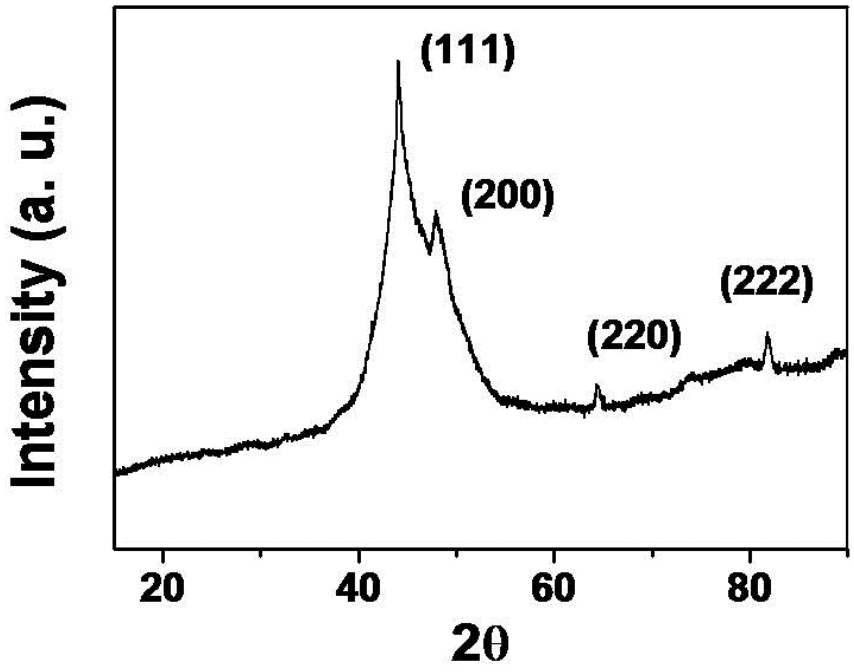


Fig. 4 X-ray diffraction pattern of nickel nanoparticles synthesised using oleylamine as the size limiting agent with 5.6×10^{-3} mols of tri-octylphosphine as the capping ligand, with a reaction temperature of 588 K and a reaction time of 240 min

Figure 3(D) displays nickel nanoparticles synthesised from the thermal decomposition of nickel acetylacetonate with oleylamine as the size limiting agent and reducing the amount of *n* –trioctylphosphine from 5.6×10^{-3} mols to 4.0×10^{-3} mols (sample Ni-6). This reduction in the amount of capping ligand present results in the growth of nickel nanoparticles from 2.8 nm to 17.8 ± 1.3 nm. This increase in nanoparticle size is expected as the amount of capping ligand present is reduced, allowing the agglomeration of an increased amount of nuclei in the growth stages of the nickel nanoparticles.

Magnetic Characterisation

The magnetic measurements concentrated on the largest and the smallest particles produced in this work, *i.e.* the 2.8 ± 0.5 nm nanoparticles (Ni-1) and the 17.8 ± 1.3 nm nanoparticles (Ni-6), synthesised from the thermal decomposition of nickel acetylacetonate in oleylamine using 5.6×10^{-3} and 4.0×10^{-3} mols of tri-octylphosphine, respectively. The magnetic properties of these two nickel nanoparticle samples were investigated by measuring both the hysteresis curves (magnetisation (M) plotted against field strength (H)) and temperature dependant magnetisation (M plotted against temperature (T)).

As the size of metal nanoparticles is reduced below their critical diameter of approximately 55 nm, the particles should become single magnetic domains (Lu et al. 2007). The magnetic properties of metal nanoparticles depend on a number of factors; for a single domain magnetic particle with a volume V at a given temperature T, the relationship between the magnetic anisotropy energy $K.V$ (where K is the magnetic anisotropy constant) and the thermal agitation $k_B.T$ (where k_B is the Boltzmann constant) will determine their potential technological applications. For biological and biomedical applications, nanoparticles which exhibit reversible magnetic behaviour at room temperature ($k_B.T >> K.V$), *i.e.* superparamagnetic, are most preferable (Dave and Gao 2009); while for data storage applications, particles must have a stable, switchable magnetic state which is unaffected by temperature fluctuations in order to represent information bits ($K.V >> k_B. T$).

The magnetic characterisation of metal nanoparticles typically involves measuring the magnetisation as the applied magnetic field is driven to saturation; and field-cooled (FC) and zero-field-cooled (ZFC) susceptibility measurements. Superparamagnetic nanoparticles generally display a blocking temperature (T_B) at which the ZFC susceptibility is at a

maximum. The ZFC and FC curves will subsequently diverge at temperatures below the blocking temperature. The metal nanoparticles will display typically ferromagnetic hysteresis loops and remnant magnetisation at temperatures below the blocking temperature and no magnetic hysteresis or remanance above the blocking temperature (Cullity and Graham 2009). This behaviour has previously been reported in the synthesis of a number of superparamagnetic materials (Min et al. 2010; Kim et al. 2009; Bala et al. 2009).

The hysteresis loops of the nickel nanoparticles with mean diameters of 2.8 and 17.8 nm at 300 K and 2 K are presented in Figures 5(A) and (B), respectively, at applied field strengths between ± 50 kOe. The inset in each figure shows the magnetisation of the samples at low applied fields. Both samples display broadly ferromagnetic hysteretic behaviour at 2 K. This broad, ferromagnetic behaviour is not observed at room temperature and this behaviour is typical of superparamagnetic nanoparticles. However, the samples are not observed to fully saturate, even at a 50 kOe applied field strength. As XRD analysis (Figure 1) indicated that the particles synthesised were metallic in nature, it is unlikely that this was due to a contribution from oxidised nanoparticles. The lack of saturation is consistent with the small grain sizes observed in the TEM images. This behaviour has previously been noted in nickel nanoparticles where similar hysteresis behaviour has been due to two contributions: a ferromagnetic contribution from nanoparticles with a grain size larger than that of the critical domain size; and a superparamagnetic contribution from the smaller nanoparticles (Mourdikoudis et al. 2009). The coercivity of the nickel nanoparticles with a mean diameter of 2.8 nm at 2 K was found to be 394 Oe and that of the 17.8 nm nanoparticles was 487 Oe. The coercivity at 300 K was approximately zero.

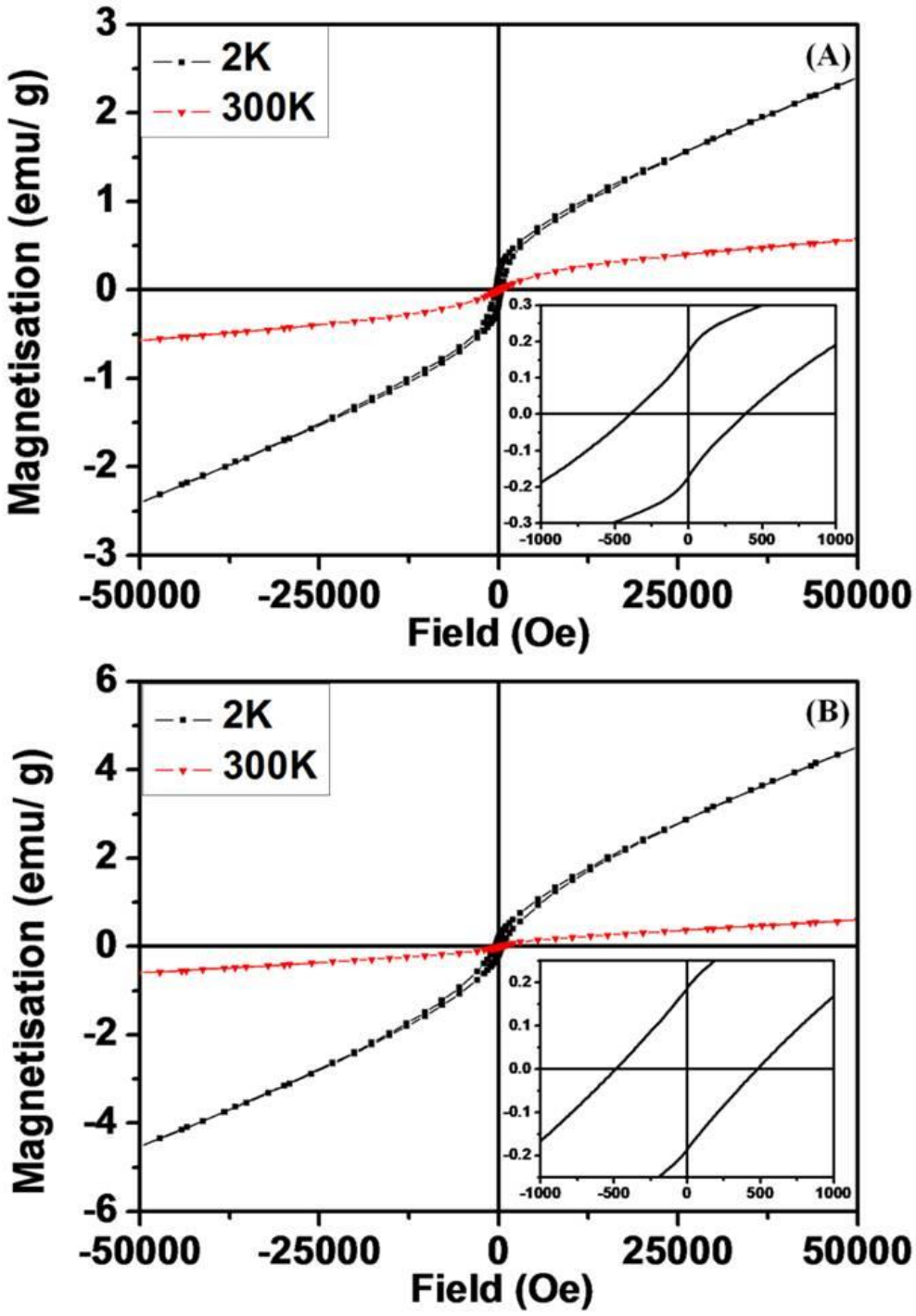


Fig. 5 Magnetisation versus applied field hysteresis loops measured at 300 K and 2 K for (A) 2.8 nm (Ni-1) and (B) 17.8 nm (Ni-6) nickel nanoparticles. The inset in each figure displays the magnetisation at reduced applied magnetic field at 2 K

In order to obtain the zero-field-cooled (ZFC) measurement, the samples were cooled to 5 K in the absence of an external field. An external magnetic field of 10 Oe was then applied to the samples and the magnetisation was measured as the temperature was increased. The samples were then immediately cooled to 5 K in the presence of the same 10 Oe magnetic field for the field-cooled (FC) portion of the measurement. The FC-ZFC magnetisation curves presented in Figures 6(A) and (B) represent the measurements taken from the Ni nanoparticles with mean diameters of 2.8 and 17.8 nm, respectively. For both samples, an effect of cooling is clearly observable. The blocking temperature of a magnetic nanoparticle can be measured at the point where the FC and the ZFC curves begin to diverge. The distinct maximums in the ZFC curves can be attributed to the blocking temperatures (T_B) of both samples. The 2.8 nm Ni nanoparticle sample was found to have a blocking temperature in the range 4.1 – 12.6 K; while the blocking temperature of the 17.8 nm sample occurred at 5.1 – 19.5 K. The blocking temperature of a nanoparticle is a size related property of single-domain ferromagnetic nanoparticles.

The blocking temperature is related to the size of the magnetic nanoparticles and the magneto-crystalline anisotropy constant (K) by the equation $K = 25.k_B.T_B/V$, where k_B and V are the Boltzmann constant and the volume of a single particle, respectively, and T_B is the blocking temperature. This equation implies that the larger the magnetic nanoparticle, the larger the blocking temperature; a trend which is observed in the magnetic properties of the two nickel nanoparticles samples measured here.

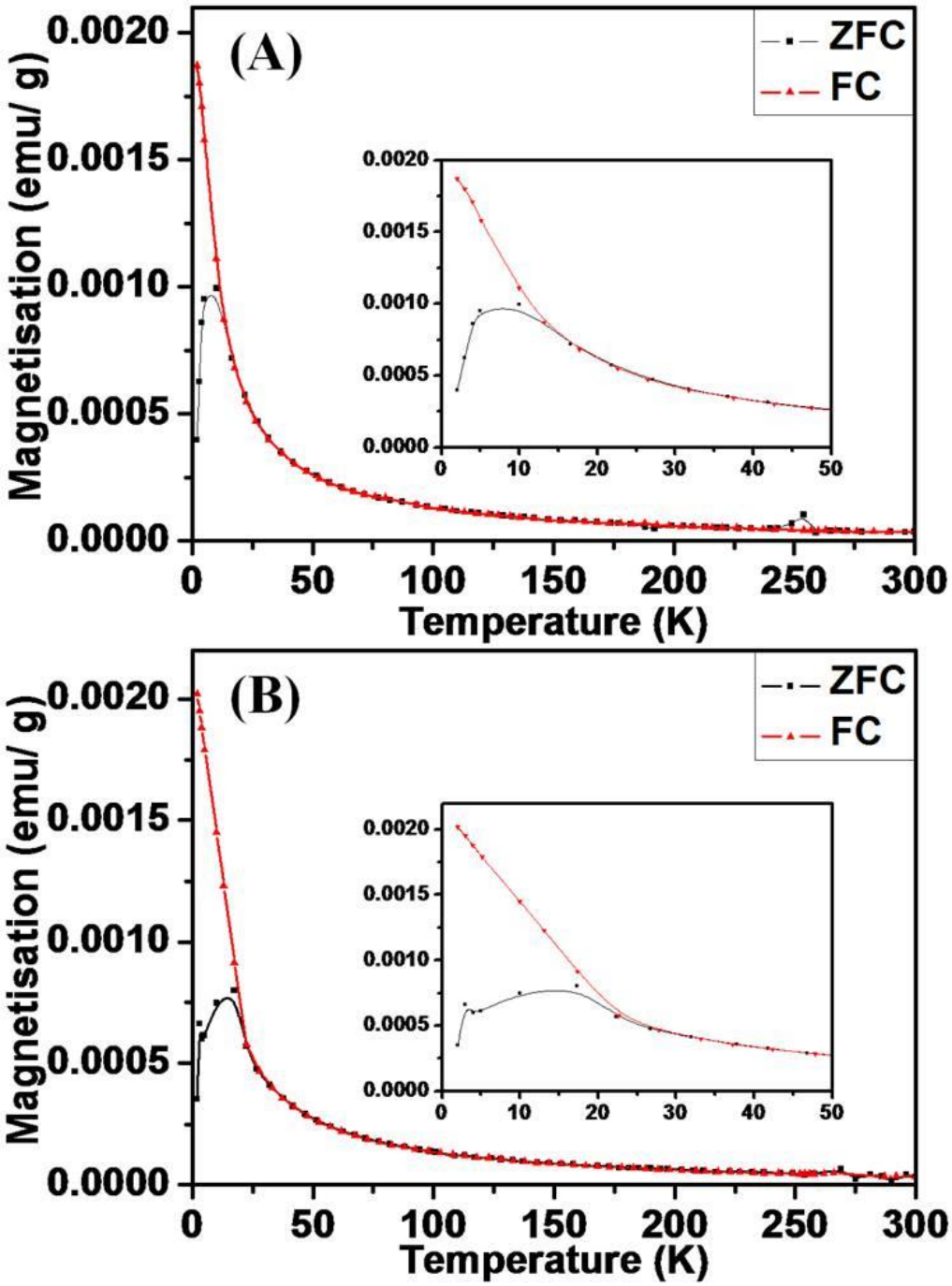


Fig. 6 Field-Cooled (FC) and Zero-Field-Cooled (ZFC) measurements taken with 10 Oe of magnetic field strength applied for (A) 2.8 nm nickel nanoparticles (Ni-1) and (B) 17.8 nm

nickel nanoparticles (Ni-6). The lower portion of each of the curves represents the ZFC measurement and the upper portion represents the FC measurement

Conclusion

While previous reports on the synthesis of nickel nanoparticles through thermal decomposition have focused on the use of various phosphines to control the size of nickel nanoparticles; or the use alkylamines to control the phase of nickel nanoparticles, this report focuses on the use of alkylamines to control the size of the nickel nanoparticles produced. In this study, the size of nickel nanoparticles has been controlled by employing various alkylamines, which are acting as the size limiting agents, and excess tri-octylphosphine, which is employed as the capping ligand. The alkylamines with bulkier chains produced nanoparticles of smaller sizes by constricting the amount of nickel nuclei available for uptake into the particle core, *i.e.* use of oleylamine resulted in nanoparticles with a mean diameter of 2.8 ± 0.5 nm in diameter; while employing *N,N*-diisopropylethylamine as the size limiting agent under the same reaction conditions produced particles with a mean diameter of 5.1 ±0.6 nm. Control of particle size was also demonstrated by increasing the time and temperature of the reaction synthesis. Increasing the reaction time from 30 to 240 min, while maintaining all other reaction conditions resulted in an increase in the mean particle size from 2.8 ± 0.9 nm to 5.1 ± 0.7 nm. By reducing the amount of capping ligand (TOP) present in the reaction medium and maintaining the reaction for 30 min at 493 K allowed further growth of the particles to 17.8 ± 1.3 nm. Magnetic characterisation of the smallest and largest nickel nanoparticles in this study, *i.e.* the 2.8 and 17.8 nm revealed both samples to be superparamagnetic in nature, with blocking temperatures of 7.9 K and 14.6 K, respectively. From this study, it can be concluded that choice of alkylamine, reaction time and reaction temperature are all important parameters in the synthesis of nickel nanoparticles *via* the

thermal decomposition of organometallic precursors. To our knowledge this is the first reported synthesis of spherical nickel nanoparticles capped with *N,N*-dimethylhexadecylamine and *N,N*-diisopropylethylamine synthesised from the thermal decomposition of organometallic precursors. The choice of metal precursor, capping ligand and solvent, together with the variation of molar ratios of these components, time and temperature of the reaction system have all been shown to have an effect on particle size, however the constant in the methods outlined in both this and previous works is the thermal decomposition of a metal precursor. This method's practicality, facile nature and ease of reproducibility, along with, as we have shown in this work, the level of size control and adaptability to include new ligands is of significant importance in the continuing exploration of the applications of metal nanoparticles.

Acknowledgements

We acknowledge financial support from Science Foundation Ireland (Project: 06/IN.1/I98). This research was also enabled by the Higher Education Authority Program for Research in Third Level Institutions (2007-2011) via the INSPIRE programme.

References

Ahmed J, Sharma S, Ramanujachary KV, Lofland SE, Ganguli AK (2009) Microemulsion-mediated synthesis of cobalt (pure fcc and hexagonal phases) and cobalt-nickel alloy nanoparticles. Journal of Colloid and Interface Science 336 (2):814-819. doi:10.1016/j.jcis.2009.04.062

Babes L, Denizot B, Tanguy G, Le Jeune JJ, Jallet P (1999) Synthesis of iron oxide nanoparticles used as MRI contrast agents: A parametric study. Journal of Colloid and Interface Science 212 (2):474-482

Bala T, Gunning RD, Venkatesan M, Godsell JF, Roy S, Ryan KM (2009) Block copolymer mediated stabilization of sub-5 nm superparamagnetic nickel nanoparticles in an aqueous medium. Nanotechnology 20 (41). doi:10.1088/0957-4484/20/41/415603

Chen YZ, Peng DL, Lin DP, Luo XH (2007) Preparation and magnetic properties of nickel nanoparticles via the thermal decomposition of nickel organometallic precursor in alkylamines. Nanotechnology 18 (50). doi:10.1088/0957-4484/18/50/505703

Cullity BD, Graham CD (2009) Introduction to Magnetic Materials. 2 edn. IEEE press, A Wiley and Sons, Inc,

Davar F, Fereshteh Z, Salavati-Niasari M (2009) Nanoparticles Ni and NiO: Synthesis, characterization and magnetic properties. Journal of Alloys and Compounds 476 (1-2):797-801. doi:10.1016/j.jallcom.2008.09.121

Dave SR, Gao XH (2009) Monodisperse magnetic nanoparticles for biodetection, imaging, and drug delivery: a versatile and evolving technology. Wiley Interdisciplinary Reviews-Nanomedicine and Nanobiotechnology 1 (6):583-609. doi:10.1002/wnan.51

Dharmaraj N, Prabu P, Nagarajan S, Kim CH, Park JH, Kim HY (2006) Synthesis of nickel oxide nanoparticles using nickel acetate and poly(vinyl acetate) precursor. Materials Science and Engineering B-Solid State Materials for Advanced Technology 128 (1-3):111-114. doi:10.1016/j.mseb.2005.11.021

Du DHC (2008) Recent Advancements and Future Challenges of Storage Systems. Proceedings of the Ieee 96 (11):1875-1886. doi:10.1109/jproc.2008.2004321

Farrell D, Majetich SA, Wilcoxon JP (2003) Preparation and characterization of monodisperse Fe nanoparticles. Journal of Physical Chemistry B 107 (40):11022-11030. doi:10.1021/jp0351831

Fievet F, Lagier JP, Blin B, Beaudoin B, Figlarz M (1989) Homogeneous and Heterogeneous Nucleations in the Polyol Process for the Preparation of Micron and Sub-Micron Size Metal Particles. Solid State Ion 32-3:198-205

Galvez N, Sanchez P, Dominguez-Vera JM, Soriano-Portillo A, Clemente-Leon M, Coronado E (2006) Apoferritin-encapsulated Ni and Co superparamagnetic nanoparticles. Journal of Materials Chemistry 16 (26):2757-2761. doi:10.1039/b604860a

Hergt R, Dutz S, Muller R, Zeisberger M (2006) Magnetic particle hyperthermia: nanoparticle magnetism and materials development for cancer therapy. Journal of Physics-Condensed Matter 18 (38):S2919-S2934. doi:10.1088/0953-8984/18/38/s26

Hyeon T, Lee SS, Park J, Chung Y, Bin Na H (2001) Synthesis of highly crystalline and monodisperse maghemite nanocrystallites without a size-selection process. Journal of the American Chemical Society 123 (51):12798-12801. doi:10.1021/ja016812s

Kim CW, Cha HG, Kim YH, Jadhav AP, Ji ES, Kang DI, Kang YS (2009) Surface Investigation and Magnetic Behavior of Co Nanoparticles Prepared via a Surfactant-Mediated Polyol Process. Journal of Physical Chemistry C 113 (13):5081-5086. doi:10.1021/jp809113h

Liu SQ, Tang ZY (2010) Nanoparticle assemblies for biological and chemical sensing. Journal of Materials Chemistry 20 (1):24-35. doi:10.1039/b911328m

Liu WT (2006) Nanoparticles and their biological and environmental applications. Journal of Bioscience and Bioengineering 102 (1):1-7. doi:10.1263/jbb.102.1

Lu AH, Salabas EL, Schuth F (2007) Magnetic nanoparticles: Synthesis, protection, functionalization, and application. Angewandte Chemie-International Edition 46 (8):1222-1244. doi:10.1002/anie.200602866

Luo XH, Chen YZ, Yue GH, Peng DL, Luo XT (2009) Preparation of hexagonal close-packed nickel nanoparticles via a thermal decomposition approach using nickel acetate tetrahydrate as a

precursor. Journal of Alloys and Compounds 476 (1-2):864-868. doi:10.1016/j.jallcom.2008.09.117
Min YL, Xia HY, Chen YC, Zhang YG (2010) Ascorbic acid-assisted synthesis of hematite microstructures and magnetic properties. Colloids and Surfaces a-Physicochemical and Engineering Aspects 368 (1-3):1-5. doi:10.1016/j.colsurfa.2010.05.039
Mourdikoudis S, Simeonidis K, Vilalta-Clemente A, Tuna F, Tsiaoussis I, Angelakeris M, Dendrinou-Samara C, Kalogirou O (2009) Controlling the crystal structure of Ni nanoparticles by the use of alkylamines. Journal of Magnetism and Magnetic Materials 321 (18):2723-2728. doi:10.1016/j.jmmm.2009.03.076
Murray CB, Sun SH, Doyle H, Betley T (2001) Monodisperse 3d transition-metal (Co, Ni, Fe) nanoparticles and their assembly into nanoparticle superlattices. Mrs Bulletin 26 (12):985-991
Pachon LD, Thathagar MB, Hartl F, Rothenberg G (2006) Palladium-coated nickel nanoclusters: new Hiyama cross-coupling catalysts. Physical Chemistry Chemical Physics 8 (1):151-157. doi:10.1039/b513587g
Park J, Kang E, Son SU, Park HM, Lee MK, Kim J, Kim KW, Noh HJ, Park JH, Bae CJ, Park JG, Hyeon T (2005) Monodisperse nanoparticles of Ni and NiO: Synthesis, characterization, self-assembled superlattices, and catalytic applications in the Suzuki coupling reaction. Advanced Materials 17 (4):429-+. doi:10.1002/adma.200400611
Roca AG, Costo R, Rebolledo AF, Veintemillas-Verdaguer S, Tartaj P, Gonzalez-Carreno T, Morales MP, Serna CJ (2009) Progress in the preparation of magnetic nanoparticles for applications in biomedicine. Journal of Physics D-Applied Physics 42 (22). doi:10.1088/0022-3727/42/22/224002
Roca AG, Morales MP, Serna CJ (2006) Synthesis of monodispersed magnetite particles from different organometallic precursors. Ieee Transactions on Magnetics 42 (10):3025-3029. doi:10.1109/tmag.2006.880111
Sun SH, Zeng H (2002) Size-controlled synthesis of magnetite nanoparticies. Journal of the American Chemical Society 124 (28):8204-8205. doi:10.1021/ja026501x
Tartaj P, Morales MD, Veintemillas-Verdaguer S, Gonzalez-Carreno T, Serna CJ (2003) The preparation of magnetic nanoparticles for applications in biomedicine. Journal of Physics D-Applied Physics 36 (13):R182-R197
Vidal-Vidal J, Rivas J, Lopez-Quintela MA (2006) Synthesis of monodisperse maghemite nanoparticles by the microemulsion method. Colloids and Surfaces a-Physicochemical and Engineering Aspects 288 (1-3):44-51. doi:10.1016/j.colsurfa.2006.04.027
Wang JP (2008) FePt Magnetic Nanoparticles and Their Assembly for Future Magnetic Media. Proceedings of the Ieee 96 (11):1847-1863. doi:10.1109/jproc.2008.2004318
Xu CJ, Sun SH (2007) Monodisperse magnetic nanoparticles for biomedical applications. Polymer International 56 (7):821-826. doi:10.1002/pi.2251
Yang H, Ito F, Hasegawa D, Ogawa T, Takahashi M (2007a) Facile large-scale synthesis of monodisperse Fe nanoparticles by modest-temperature decomposition of iron carbonyl. Journal of Applied Physics 101 (9). doi:09j112

10.1063/1.2711391
Yang HT, Ito F, Hasegawa D, Ogawa T, Takahashi M (2007b) Facile large-scale synthesis of monodisperse Fe nanoparticles by modest-temperature decomposition of iron carbonyl. Journal of Applied Physics 101 (9). doi:09j112

10.1063/1.2711391
Yang HT, Shen CM, Wang YG, Su YK, Yang TZ, Gao HJ (2004) Stable cobalt nanoparticles passivated with oleic acid aind triphenylphosphine. Nanotechnology 15 (1):70-74. doi:10.1088/0957-4484/15/1/014
Yu WW, Falkner JC, Yavuz CT, Colvin VL (2004) Synthesis of monodisperse iron oxide nanocrystals by thermal decomposition of iron carboxylate salts. Chemical Communications (20):2306-2307. doi:10.1039/b409601k

Zhang HT, Chen XH (2005) Controlled synthesis and anomalous magnetic properties of relatively monodisperse CoO nanocrystals. Nanotechnology 16 (10):2288-2294. doi:10.1088/0957-4484/16/10/051

Zhu YH, Stubbs LP, Ho F, Liu RZ, Ship CP, Maguire JA, Hosmane NS (2010) Magnetic Nanocomposites: A New Perspective in Catalysis. Chemcatchem 2 (4):365-374. doi:10.1002/cctc.200900314